

Near-Ambient Pressure Velocity Map Imaging

Tzu-En Chien, Lea Hohmann, and Dan J. Harding^{a)}

Dept. of Chemical Engineering, KTH Royal Institute of Technology, Stockholm 100 44, Sweden

(Dated:)

We present a new velocity map imaging instrument for studying molecular beam surface scattering in a near-ambient pressure (NAP-VMI) environment. The instrument offers the possibility to study chemical reaction dynamics and kinetics where higher pressures are either desired or unavoidable. NAP-VMI conditions are created by two sets of ion optics that guide ions through an aperture and map their velocities. The aperture separates the high pressure ionization region and maintains the necessary vacuum in the detector region. The performance of the NAP-VMI is demonstrated with results from N₂O photodissociation and N₂ scattering from Pd(110) surface, which are compared under vacuum and at near-ambient pressure (1×10^{-3} mbar). NAP-VMI has the potential to be applied to, and useful for, a broader range of experiments including photoelectron spectroscopy and scattering with liquid microjets.

INTRODUCTION

Particle imaging techniques based on Ion Imaging¹ and Velocity Map Imaging (VMI)² have revolutionized the field of chemical dynamics, allowing very efficient collection of the velocity distributions of particles coming from a variety of processes. (photodissociation,¹⁻³ photoelectron spectroscopy,^{2,4,5} inelastic⁶⁻⁸ and reactive scattering⁹) Charged particle-neutral collisions can also be probed¹⁰⁻¹² The velocity distributions provide information about the physics underlying and controlling the process of interest. The high collection efficiency is particularly valuable for time-resolved experiments, where many measurements need to be made, and for low count rate experiments.

Imaging techniques are still in very active development. Hardware is being pushed in different directions to give ion optics with higher energy resolution^{2,13,14}, larger energy acceptance,¹⁵⁻¹⁸ or smaller sizes.¹⁹ Efforts are also ongoing to develop faster, more flexible, and more accurate image reconstruction methods.²⁰⁻²⁴

Many of these developments are related to the fact that during the imaging detection process a 3D-distribution of particles is projected onto a 2D-detector. There are different approaches to deal with this, depending largely on the nature of the experiment. The most common way, if the experimental set-up has suitable symmetry, is to apply an inverse-Abel transform to the 2D image to recover the original 3D distribution. For systems without this symmetry there are several options including: 3D imaging where the position and arrival time of each particle is measured,²⁵ recently extended to electrons by the use of the TPX3CAM fast camera.²⁶ Time slicing approaches, which use more complex electric fields to spread the ions' arrival times at the detector allowing only a chosen section of the ion distribution to be imaged.²⁷⁻³² There are also options to spatially select the particles that are detected by laser slicing, where only a subset of the scatter-

ing products are ionized,³³ or space slice imaging, where the ions are selected with physical slit before being accelerated perpendicularly on to a detector.³⁴

Additional optical elements have also been used to zoom in or out on images. In particular, Offerhaus et al., used an einzel lens as a magnifier for PEI,³⁵ which had a hard focus, or crossover, similar to that reported here. Due to the different application, it was much further from the extraction region.

These strengths of imaging detection have recently been applied to molecular beam surface scattering experiments, where they can be used to probe the dynamics of the molecule-surface interactions^{36,37} Using pulsed molecular beams and lasers even allows pump-probe measurements of the kinetics of surface processes and reactions by directly probing the time-dependent flux of molecules leaving the surface.³⁸⁻⁴⁰ Wodtke and co-workers are developing high repetition rate imaging experiments that can probe the time dependence within a single MB pulse, and will allow changes in the surface during reaction to be investigated.⁴¹

Typically, the pressure in the extraction region of an imaging system must be kept in the high vacuum region (below 1×10^{-6} mbar) to avoid collisions of the particles with background gas and to prevent electrical arcing on the ion optics, or worse, the microchannel plate(s) and phosphor screen of the detector. For experiments on gas phase molecules these pressure requirements do not typically pose a problem and the normal solution of well defined molecular beams also improve other aspects of the experiment (e.g. energy resolution in scattering experiments, well defined interaction region). When studying gas-solid or gas-liquid interfaces there are many cases where it is not possible or desirable to work in such high vacuum, either because the condensed phase has too high a vapor pressure (e.g. volatile liquids) or because the surface is changed by the presence of reactive gases. This has led to the development of instrumentation to allow 'high-vacuum' techniques to be applied at higher pressures. The names given to these different adaptations depend upon the field, but in general use some combina-

^{a)}Electronic mail: djha@kth.se

tion of confining the high pressure region while allowing the particles of interest to reach a detector without losing the useful information they carry. The surface science community has long recognized the importance of the reactant gas pressure in changing the structure and properties of surfaces, known as the ‘pressure gap’ between ultrahigh vacuum (UHV) and applied catalysis.^{42–44} In order to help close the gap it is also important to be able to switch rapidly between UHV and high(er) pressure.

We will briefly review some areas where surface methods detecting charged particles have been extended to higher pressure and which are closely related from their technology and/or applications to the NAP-VMI we describe here.

One of the most widely used techniques for fundamental catalysis research is photoelectron spectroscopy (PES), and there have been significant efforts starting in the 1970s and taking off in the early 2000s to allow PES to be performed at higher ‘near-ambient’ and ambient pressures.^{45,46} In the early instruments small apertures and differential pumping were used to separate the interaction region from the analyzer and maintain suitable vacuum. The use of electron lenses in the differential pumping region allowed higher transmission and pressures.⁴⁷ The addition of reaction cells⁴⁸ and, most recently, developments using virtual cells have pushed the achievable surface pressure above 1 bar.⁴⁹ Time resolved APXPS experiments have also been developed^{50,51} and experiments with time resolution of 50 ms have very recently been reported.⁵² AP-XPS instruments also provide means to measure the gas composition in front of the surface, with XPS, and in the bulk gas mixture, with mass spectrometer(s), which allows the surface composition to be linked to the reactivity. Care must be taken in using mass spectrometry (MS) as comparison of NAP-XPS, Planar Laser Induced Florescence (PLIF) and MS shows that the composition directly in front of the surface is different to the average composition in the reactor, which is what is sampled by MS in most cases.^{46,53} These features have allowed AP-XPS to make huge advances in determining the chemical species that are present during reactions at elevated pressure and identifying which are the most reactive. The time resolved measurements are moving towards direct measurement of the surface reaction kinetics but, to our knowledge, these have not been reported so far.

Liquid-gas interfaces are another important area for chemistry where high pressures of gas are often unavoidable, due to evaporation of the liquid. Experiments to probe the scattering and evaporation of molecules from liquid surfaces, i.e. measurements of the residence times of atoms and molecules on the surface and/or velocity distributions with which they leave, can provide information about the processes occurring at the interface and the liquid surface composition and structure.^{54,55} For low vapor pressure liquids, a partially submerged wheel rotating through the liquid can be used to produce a continuously clean surface. Techniques similar to

those used for gas-solid scattering can then be used.^{56–59} Recently, VMI has been also applied to MB scattering from SAMs on metal surfaces.^{60,61} Liquid metals can also have sufficiently low vapor pressure to be studied with MB methods similar to those for the solids, providing information about energy transfer processes.⁶² Liquid microjets⁶³ have made it possible to study evaporation from volatile liquids^{63,64} and molecular beam scattering from salty water.⁶⁵

The Environmental Molecular Beam (EMB) technique, which has been developed in Gothenburg to allow scattering experiments from volatile liquids, uses an aperture or a grating to separate the high pressure surface from the low pressure detector region.^{66,67} This allows high pressure and very short flight distances of the molecules through the high pressure region. The use of electron ionization provides universal detection but prevents quantum state specific measurements. Compared to imaging detection, this design can measure only one angle at a time and the data analysis is more complicated, particularly to separate surface residence time distributions from the molecular speed distribution.⁶⁸

As for solid surfaces, photoelectron spectroscopy can provide information about the liquid surface. The gas load in the system can be reduced by the use of liquid microjets^{63,69} which, when combined with AP-XPS analyzers, allow photoelectron spectroscopy of liquid interfaces.^{70,71} Developments in the area are being driven by the desire to gain more information from the emitted photoelectrons. Interest in the angular distribution of the slow photoelectrons, particularly for measurements of circular dichroism, has led to the development of an instrument combining a liquid jet with movable analyzer⁷² and a very recent report of a VMI set up to probe the angular distribution.⁷³ Tesa-Serate et al.,⁵⁴ suggested that more ‘more sophisticated imaging methods for detecting the scattered products’ will be useful for molecular beam liquid surface experiments.

Here, we present a new instrument developed to allow velocity map imaging of molecular beam (MB) surface scattering and reactions occurring at near-ambient pressure (NAP-VMI). Very high resolution velocity is not a requirement for imaging detection to be useful for surface scattering experiments as, even starting with very well defined beams e.g. ref⁷⁴, most surface scattering processes from metals produce rather broad distributions. Despite this, dynamic fingerprints can still be observed in scattering distributions which can help to separate different processes or reaction channels.^{39,75} We expect this to be the case for the reactive scattering we intend to study.

We will describe the NAP-VMI ion optics and show tests of the set up using the well characterized photodissociation of gas-phase N_2O , and MB scattering of N_2 from Pd(110) at pressures up to 1×10^{-3} mbar. The NAP-VMI can be run in two different modes of operation, one as a ‘classical’ three electrode VMI² and a second mode, using two sets of electrodes with a crossover of the

ions at the aperture which provides DC slicing^{28,29}. This mode has the potential to allow even higher pressures by allowing smaller apertures, lower extraction voltages in the high pressure region, and additional stages of differential pumping by refocusing the particles through more apertures, similar to many current AP-XPS analyzers.

Our NAP-VMI instrument enables unique state-resolved gas-solid MB scattering experiments and we suggest that the method has the potential to be interesting and useful to a much broader range of the chemical dynamics community. The acceptable pressure in interaction region should allow MB scattering from volatile liquid surfaces or liquid jets and, as Long et al. very recently demonstrated, angular information from liquid jet PES.⁷³ Some of the features of our implementation may be particularly useful for LJ-PES and LJ-PECD, in particular, the small aperture size would allow the use of flatjet, providing a better defined system for angular measurements⁷⁶ and allow all photoelectrons to be probed simultaneously. In the crossing mode, the low voltage on the first electrode stack might also reduce the problems with electric breakdown that Long et al. describe for their implementation.⁷³

METHODS

A. Overall design

Figure 1 shows the schematic diagram of the apparatus. It consists of a molecular beam source chamber, scattering chamber, detection chamber, sample preparation chamber and laser system. The scattering and detector chambers are pumped by 300 l/s and 80 l/s turbomolecular pumps, respectively. A top hat shaped flange is installed between them. A 3 mm aperture on the top hat separates the chambers, providing differential pumping and allowing pressure differences of a factor of 1000 to be maintained. Electrodes on either side of the aperture provide the fields needed for velocity mapping.

The instrument is controlled by home made Python software which controls the camera, BNC delay generator, and laser wavelength. Different types of experiment can be performed allowing integration over the speed distribution of the molecular beam or kinetic scans, where an image is saved for each MB-laser delay, needed to perform Velocity Resolved Kinetics measurements³⁸. Image manipulation is performed using the PyAbel package²³ in Python.

B. Molecular beam

The molecular beam source consists of two chambers which are separated by a skimmer (Beam Dynamics Inc., Model 1 with 2 mm opening). Source chamber and differential chamber are pumped by 350 l/s and 90 l/s turbomolecular pump, respectively. A pulsed valve (Ams-

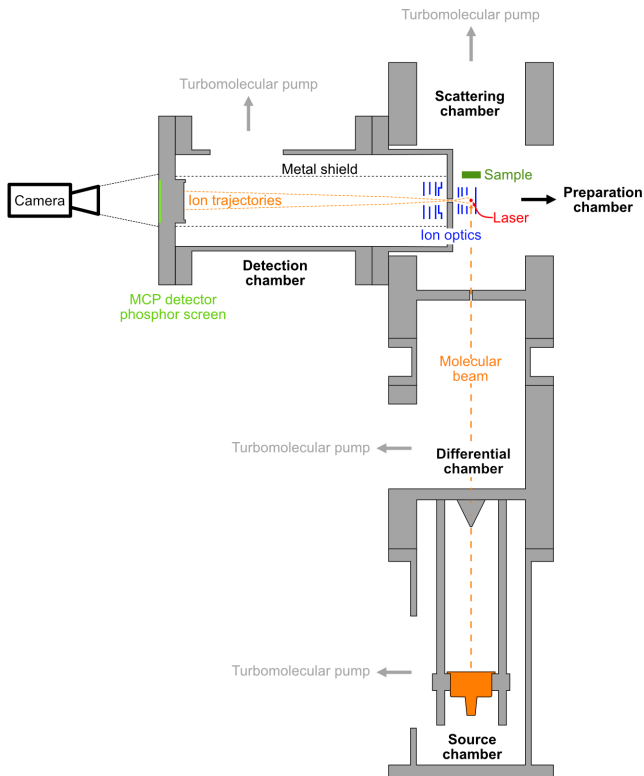


FIG. 1. Schematic diagram of the NAP-VMI apparatus.

terdam Piezo Valve) is mounted in the source chamber which runs at 10 Hz repetition rate with a pulse width between 20-100 μ s. The molecular beam source is mounted below the scattering chamber, separated by a 1 mm aperture. With the pulsed valve in operation the pressure of the source chamber increases to 1×10^{-5} mbar, the pressure of the differential chamber increases to 1×10^{-7} mbar, and the pressure of the scattering chamber is unchanged.

C. Detector chamber

The detector chamber is pumped by a 70 l/s turbomolecular pump. A 40 mm Z-stack MCP and P43 phosphor screen (Photek) is used. The ion cloud is sliced by applying a short pulse of -500V to the front MCP. Light from the phosphor screen is then captured by a CCD camera (FLIR, 1.3 megapixel) with an 8 mm lens. The ion flight distance is 260 mm. A metal grid is used to shield the field free flight region from the high voltage feedthroughs in the detector chamber.

D. VMI ion optics

In order to minimize scattering with background gas under NAP conditions the distance from the surface to the ionization region must be kept small. Consequently, the electrodes for the VMI optics also need to be small. The small size of the ion optics makes it more difficult to achieve high velocity resolution imaging compared to a larger set-up; for given voltages, the field gradients are larger, the ionization volume of the laser is a larger fraction of the extraction region, and mechanical imperfections are more important. The weak extraction fields we use should increase the volume over which VMI conditions are met.⁷⁷

Figure 2 shows the VMI ion optics setup. It consists of eight 1 mm thick stainless steel electrodes. The first set of four electrodes (R, E1, E2, G) are designed to produce a hard focus of the ions at the aperture on the top hat. The second set of four electrodes (F1, F2, F3, F4) function as an acceleration region and an Einzel lens that fine tunes the focusing. Electrode R is a solid rectangle (85 mm x 18 mm), electrodes E1, E2, and E3 are rectangular plate (52 mm x 18 mm) with 10 mm, 8 mm and 6 mm hole in the center, respectively. The distance between electrodes R, E1, E2, G are 5 mm, 4 mm and 2 mm; the distance between electrode G and the top hat flange is 5 mm and the wall thickness of the top hat is 6 mm. F1 electrode is a square plate (25 mm x 25 mm) with concentric circles extrusion (18 mm outer diameter and 16 mm inner diameter) forming a shape of a top hat and have a 6 mm hole in the center. Electrodes F2, F3 and F4 are square plate (25 mm x 25 mm) with 6 mm, 8 mm and 6 mm hole in the center, respectively. The distance between the top hat flange, F1, F2, F3 and F4 are 3 mm. Figure 3 shows the electric field and ion trajectory simulation of N_2^+ ions with kinetic energy of 0.03 eV, 0.27 eV and 0.75 eV in COMSOL Multiphysics 5.4. Ions start from the center of R and E1 electrodes and 1 and 2 mm along the laser propagation direction. Eight initial directions parallel to the imaging plane with 45 degrees spacing were considered. The simulated voltages on R, E1, E2, G, F1, F2, F3 and F4 are 500 V, 480 V, 40 V, 0 V, -3000 V, -1500 V, 0 V, -1500 V, respectively. The ion optics also have a DC-slicing effect,^{28,29} spreading the arrival time at the detector for particles depending on their motion in the z-axis (towards the detector). Using fast gated MCPs allows only the center section of the image to be recorded, removing the need for an inverse-Abel transform. For surface scattering experiments there is also a laser slicing effect³³ due to the distance from the scattering surface to the ionization point (typically 14 mm). The out-of-plane angular acceptance is mainly determined by the size of the molecular beam at the surface and we estimate that for the ca. 3 mm beam only molecules within $\pm 15^\circ$ of the scattering plane parallel to the electrodes and detector will be ionized and these molecules will have apparent in-plane velocities up to 5% too low. For most surface scattering experiments this

is acceptable, but it could probably be improved using image analysis procedures similar to the FINA methods developed by Suits and co-workers²²

A second mode of operation, using only the first electrode stack as 3-electrode VMI is also possible, despite the small size of the aperture. This mode is very similar to the optics described by Long et al. for PEI from a liquid microjet.

The aperture has the additional benefit of effectively shielding the detector from light in the scattering chamber, which can come from scattering of the ionization laser, emission from the sample heater, or ionization filaments.

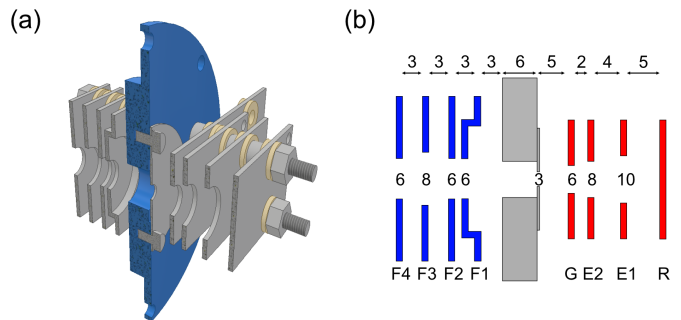


FIG. 2. (a) The cross section and (b) the construction diagram of the ion optics.

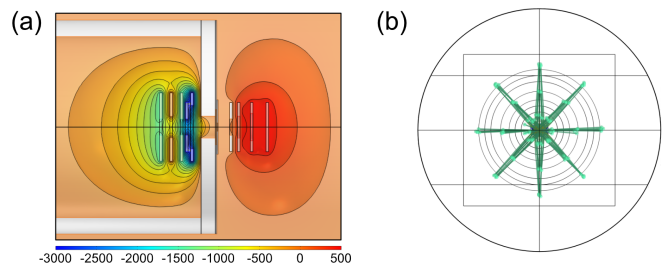


FIG. 3. Simulation of (a) electric field and (b) ion trajectory for the VMI set-up

E. Laser system

The ionization laser is generated by doubled Nd:YAG laser (InnoLas) pumped dye laser (Radiant Dyes) The DCM dye fundamental around 609 nm is frequency tripled with two BBO crystals. The laser operates at a repetition rate of 10 Hz. A variable wave plate controls

the laser beam polarization and it is focused in the center of the VMI optics by a 200 mm focal length lens.

F. Preparation chamber

The preparation chamber is pumped by a 400 l/s turbomolecular pump with a base pressure below 2×10^{-9} mbar. It contains a sputter gun (PREVAC), Auger Electron Spectrometer (RBD Instruments) and sample stage. The sample manipulator is controlled by UHV compatible linear translation and rotation stages (Arun Microelectronics Ltd.) allowing the sample to be located between sputtering, Auger and scattering regions. Prior to surface scattering experiments, the Pd(110) crystal was cleaned by argon ion sputtering for 5 min and annealed at 1000 K. Surface cleanliness was checked by Auger spectroscopy.

RESULTS AND DISCUSSION

A. N₂O photodissociation

To test and demonstrate the capabilities of the NAP-VMI optics, we have studied the well characterized photodissociation of N₂O. Photodissociation of N₂O around 203 nm produces highly rotationally excited N₂ fragments which can be detected state selectively using (2+1) REMPI.^{78–82} The different final rotational states have significantly different translational kinetic energies, providing a good system to calibrate the new imaging optics. The optimized voltages of ion optics are experimentally set at 500 V, 480 V, 400 V, 0 V, -3000 V, -1000 V, -100 V, -1000 V for R, E1, E2, G, F1, F2, F3 and F4 electrodes, respectively. Figure 4 shows a DC sliced velocity map image of N₂ ($J=74$) fragments from N₂O dissociation under high vacuum (5×10^{-9} mbar: left panel) and near-ambient pressure (1×10^{-3} mbar of Ar: right panel). Figure 5 shows the speed distribution obtained from Figure 4, the curve was used to calibrate the detector, yielding a value of 11.5 m/s per pixel. The full width at half maximum height of the peak is around 8%. Compared to other imaging systems designed for photodissociation experiments⁸¹ the speed resolution is not very high, and we are unable to resolve dissociation from different initial vibrational states of N₂O. This is presumably due to a combination of the small size of the optics and the fact that the molecular beam is parallel to the detector plane. The N₂ speeds measured for different final rotational states are shown in Figure 6. Comparison with calculated and published values^{81,82} for other final- J states shows good agreement. The measured angular distributions are also consistent with previous reports.⁸⁰ At near-ambient pressure, collisions with the background Ar reduced the total signal and broadened the speed distribution (by factors around 3 in this case) but the useful, dynamical, information is still clearly visible.

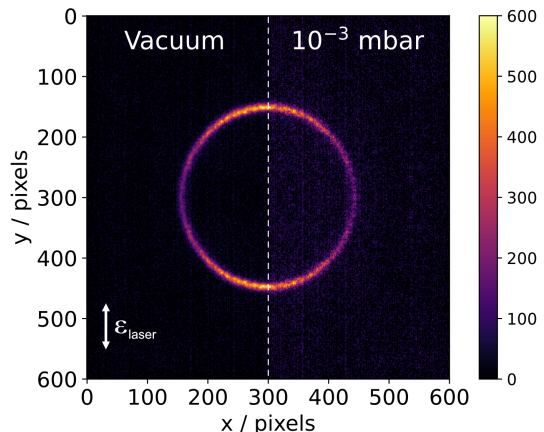


FIG. 4. DC sliced images of N₂ ($J=74$) fragments from N₂O dissociation under high vacuum: 5×10^{-9} (left panel) and near-ambient pressure: (1×10^{-3} mbar of Ar(right panel). The vertical arrow indicates the laser polarization (ϵ_{laser}) direction.

B. N₂ scattering from the Pd(110) surface

We have tested the ability of the NAP-VMI optics to probe surface scattering by measuring inelastic scattering of N₂ from Pd(110) at 300 K under ultrahigh vacuum and in a near-ambient environment in argon. The sample was placed 5 mm from the edge of the ion optics, making a 14 mm distance from sample to ionization center. We choose this distance as it reduces perturbations to the imaging fields due to the presence of the surface. The ion optics are experimentally set at 500, 480, 400, 0, -3000, -1000, -75, -1000 V for R, E1, E2, G, F1, F2, F3 and F4 electrodes, respectively. N₂ molecules are detected state selectively using (2+1) REMPI.⁸³ Figure 7 shows the velocity map images of N₂ scattering from Pd(110) under vacuum and near-ambient environment (1×10^{-3} mbar of argon). The green cross in the image center represents the thermal background of N₂ molecules, which we also use as a zero-velocity point; the upper signal ($V_x > 0$) is the incident beam which is travelling upward (approaching surface), and the lower signal ($V_x < 0$) belongs to scattering molecules which are travelling downward (leaving surface) after scattering. The images were recorded while scanning the delay between the pulse valve and the laser from 300 μ s to 800 μ s with an interval of 10 μ s, so that the full velocity distribution of molecules in the beam is included. Figure 8 shows the speed distribution from VMI images, by integrating the radius over 20° sectors centered on the incident beam and the scattered molecules direction, and angular distribution of scattered molecules. Comparing the speed distribution between high vacuum and near-ambient environment, no significant difference is found. The root mean square speed for the incident beam is 910 m/s (0.12 eV) and scattered N₂ is 535 m/s (0.042 eV), the scattered N₂

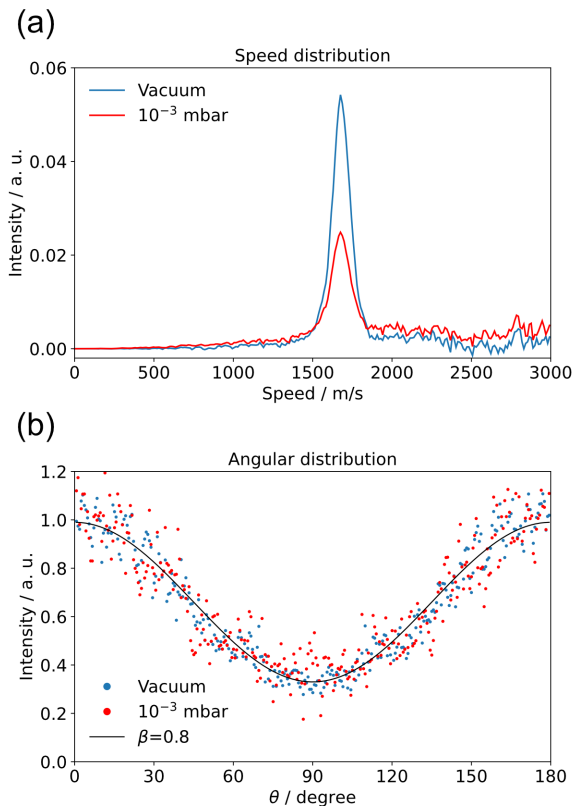


FIG. 5. (a) Speed distribution and (b) angular distribution of N_2 fragments obtained from Figure 4

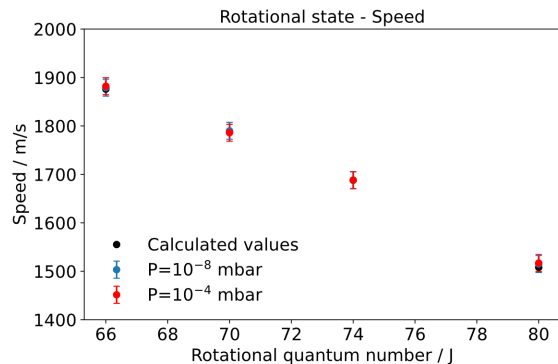


FIG. 6. Plot of mean recoil speed for different final-J states under vacuum and medium pressure (1×10^{-4} mbar of argon). The error bar was estimated to be 3 pixels (~ 35 m/s).

has lost around 65% of its kinetic energy. The observed energy loss is in good agreement with the Baule limit,⁸⁴ where the final translational energy is predicted by a hard cube model. The final translational energy $\langle E_f \rangle$, is described as $\langle E_f \rangle = \langle E_i \rangle \left(\frac{m_{Pd} - m_{N_2}}{m_{Pd} + m_{N_2}} \right)^2$, and it predicts a 66% energy loss for N_2 scattering from Pd surface. The

angular distribution for scattered N_2 is broader in the near-ambient argon environment, which we attribute to collisions with Ar atoms.

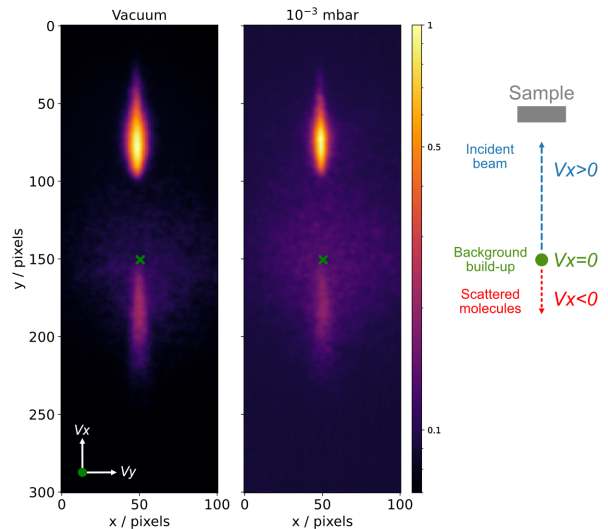


FIG. 7. Velocity-map images for N_2 scattering from Pd(110) surface ($T_s = 300$ K) under vacuum and 1×10^{-3} mbar of argon. The schematic illustration of sample, incident beam, background build-up, and scattered molecules are shown next to the images.

CONCLUSION

We have demonstrated a new instrument capable of studying molecular beam surface scattering under near-ambient pressure, providing a new tool to help close the ‘pressure gap’ in the studies of catalytic reaction. The design is based on a velocity-map image set-up that uses two sets of electrodes to focus the ions at an aperture. By putting the aperture between scattering and detector chamber, we created a differential pumping, and allow us operate under near-ambient pressure in the scattering chamber without damaging the detector. Higher pressures could be achieved by using a smaller aperture and adding additional differential pumping stages. The speed resolution is not very high, due to the compact design of the electrodes, but it reduces the number of background collision and preserves the dynamical scattering information about the reaction. This technique may be applied in a range of other areas where higher pressures are either interesting or unavoidable, e.g. liquid jets and gas-liquid interfaces

ACKNOWLEDGMENT

We acknowledge the financial support of the Swedish Foundation for Strategic Research (SSF) (ITM17-0236).

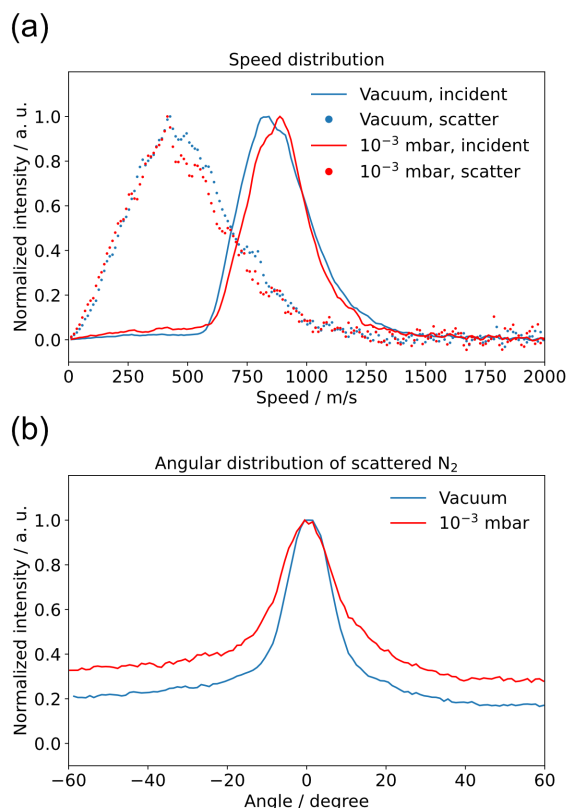


FIG. 8. (a) Speed distributions from VMI images for incident beam and scattered molecules, and (b) angular distribution for scattered N_2 .

We thank Henrik Öström for the loan of the Pd(110) crystal. DJH thanks Alice Schmidt-May for carefully reading the manuscript.

- ¹D. W. Chandler and P. L. Houston, "Two-dimensional imaging of state-selected photodissociation products detected by multiphoton ionization," *J. Chem. Phys.* **87**, 1445–1447 (1987).
- ²A. T. Eppink and D. H. Parker, "Velocity map imaging of ions and electrons using electrostatic lenses: Application in photoelectron and photofragment ion imaging of molecular oxygen," *Rev. Sci. Instr.* **68**, 3477–3484 (1997).
- ³A. G. Suits, "Invited review article: Photofragment imaging," *Rev. Sci. Instr.* **89**, 111101 (2018), <https://doi.org/10.1063/1.5045325>.
- ⁴A. S. Chatterley, C. W. West, V. G. Stavros, and J. R. R. Verlet, "Time-resolved photoelectron imaging of the isolated deprotonated nucleotides," *Chem. Sci.* **5**, 3963 (2014).
- ⁵M. L. Weichman and D. M. Neumark, "Slow photoelectron velocity-map imaging of cryogenically cooled anions," *Ann. Rev. Phys. Chem.* **69**, 101–124 (2018), PMID: 29401036.
- ⁶S. N. Vogels, J. Onvlee, S. Chefdeville, A. van der Avoird, G. C. Groenenboom, and S. Y. T. van de Meerakker, "Imaging resonances in low-energy no-he inelastic collisions," *Science* **350**, 787–790 (2015), <https://www.science.org/doi/pdf/10.1126/science.aad2356>.
- ⁷C. G. Heid, V. Walpole, M. Brouard, P. G. Jambrina, and F. J. Aoiz, "Side-impact collisions of ar with no," *Nature Chemistry* **11**, 662–668 (2019).

- ⁸T. de Jongh, M. Besemer, Q. Shuai, T. Karman, A. van der Avoird, G. C. Groenenboom, and S. Y. T. van de Meerakker, "Imaging the onset of the resonance regime in low-energy no-he collisions," *Science* **368**, 626–630 (2020), <https://www.science.org/doi/pdf/10.1126/science.aba3990>.
- ⁹H. Pan, S. Liu, D. H. Zhang, and K. Liu, "From reactive rainbow to dynamic resonance well," *J. Phys. Chem. Lett.* **11**, 9446–9452 (2020).
- ¹⁰E. Carrascosa, J. Meyer, and R. Wester, "Imaging the dynamics of ion–molecule reactions," *Chem. Soc. Rev.* **46**, 7498–7516 (2017).
- ¹¹J. Meyer, V. Tajti, E. Carrascosa, T. Györi, M. Stei, T. Michaelsen, B. Bastian, G. Czako, and R. Wester, "Atomistic dynamics of elimination and nucleophilic substitution disentangled for the $F^- + CH_3CH_2Cl$ reaction," *Nature Chemistry* **13**, 977–981 (2021).
- ¹²J. N. Bull, J. W. L. Lee, and C. Vallance, "Quantification of ions with identical mass-to-charge (m/z) ratios by velocity-map imaging mass spectrometry," *Phys. Chem. Chem. Phys.* **15**, 13796–13800 (2013).
- ¹³E. Wrede, S. Laubach, S. Schulenburg, A. Brown, E. R. Wouters, A. J. Orr-Ewing, and M. N. R. Ashfold, "Continuum state spectroscopy: A high resolution ion imaging study of IBr photolysis in the wavelength range 440–685 nm," *J. Chem. Phys.* **114**, 2629–2646 (2001), <https://doi.org/10.1063/1.1337049>.
- ¹⁴V. Plomp, Z. Gao, and S. Y. van de Meerakker, "A velocity map imaging apparatus optimised for high-resolution crossed molecular beam experiments," *Mol. Phys.* **119**, e1814437 (2021).
- ¹⁵D. A. Horke, G. M. Roberts, J. Lecointre, and J. R. R. Verlet, "Velocity-map imaging at low extraction fields," *Rev. Sci. Instr.* **83**, 063101 (2012), <https://doi.org/10.1063/1.4724311>.
- ¹⁶S. Skruszewicz, J. Passig, A. Przystawik, N. Truong, M. Köther, J. Tiggesbäumker, and K.-H. Meiwes-Broer, "A new design for imaging of fast energetic electrons," *Int. J. Mass Spectrom.* **365**, 338–342 (2014).
- ¹⁷N. G. Kling, D. Paul, A. Gura, G. Laurent, S. De, H. Li, Z. Wang, B. Ahn, C. Kim, T. Kim, *et al.*, "Thick-lens velocity-map imaging spectrometer with high resolution for high-energy charged particles," *JINST* **9**, P05005 (2014).
- ¹⁸D. Schomas, N. Rendler, J. Krull, R. Richter, and M. Mudrich, "A compact design for velocity-map imaging of energetic electrons and ions," *J. Chem. Phys.* **147**, 013942 (2017).
- ¹⁹E. Sakkoula, B. van Oorschot, and D. Parker, "A compact electrostatic lens for velocity map imaging experiments," *Mol. Phys.*, e1910357 (2021).
- ²⁰S. Manzhos and H.-P. Looock, "Photofragment image analysis via pattern recognition," *Rev. Sci. Instr.* **75**, 2435–2445 (2004).
- ²¹G. M. Roberts, J. L. Nixon, J. Lecointre, E. Wrede, and J. R. R. Verlet, "Toward real-time charged-particle image reconstruction using polar onion-peeling," *Rev. Sci. Instr.* **80**, 053104 (2009), <https://doi.org/10.1063/1.3126527>.
- ²²J. O. F. Thompson, C. Amarasinghe, C. D. Foley, N. Rombes, Z. Gao, S. N. Vogels, S. Y. T. van de Meerakker, and A. G. Suits, "Finite slice analysis (fina) of sliced and velocity mapped images on a cartesian grid," *J. Chem. Phys.* **147**, 074201 (2017), <https://doi.org/10.1063/1.4986966>.
- ²³D. D. Hickstein, S. T. Gibson, R. Yurchak, D. D. Das, and M. Ryazanov, "A direct comparison of high-speed methods for the numerical abel transform," *Rev. Sci. Instr.* **90**, 065115 (2019).
- ²⁴C. Sparling, A. Ruget, J. Leach, and D. Townsend, "Arbitrary image reflation: A deep learning technique for recovering 3d photoproduct distributions from a single 2d projection," *Rev. Sci. Instr.* **93**, 023303 (2022), <https://doi.org/10.1063/5.0082744>.
- ²⁵A. Chichinin, K.-H. Gericke, S. Kauczok, and C. Maul, "Imaging chemical reactions–3d velocity mapping," *Int. Rev. Phys. Chem.* **28**, 607–680 (2009).
- ²⁶C. Cheng, G. Moğol, T. Weinacht, A. Nomerotski, and C. Trallero-Herrero, "3d velocity map imaging of electrons with tpx3cam," *Rev. Sci. Instr.* **93**, 013003 (2022).

- ²⁷C. R. Gebhardt, T. P. Rakitzis, P. C. Samartzis, V. Ladopoulos, and T. N. Kitsopoulos, "Slice imaging: A new approach to ion imaging and velocity mapping," *Rev. Sci. Inst.* **72**, 3848–3853 (2001).
- ²⁸D. Townsend, M. P. Minitti, and A. G. Suits, "Direct current slice imaging," *Rev. Sci. Inst.* **74**, 2530–2539 (2003).
- ²⁹J. J. Lin, J. Zhou, W. Shiu, and K. Liu, "Application of time-sliced ion velocity imaging to crossed molecular beam experiments," *Rev. Sci. Inst.* **74**, 2495–2500 (2003).
- ³⁰V. Papadakis and T. N. Kitsopoulos, "Slice imaging and velocity mapping using a single field," *Rev. Sci. Inst.* **77**, 083101 (2006).
- ³¹M. Ryazanov and H. Reisler, "Improved sliced velocity map imaging apparatus optimized for H photofragments," *J. Chem. Phys.* **138**, 144201 (2013).
- ³²F. Allum, R. Mason, M. Burt, C. S. Slater, E. Squires, B. Winter, and M. Brouard, "Post extraction inversion slice imaging for 3D velocity map imaging experiments," *Mol. Phys.* **119**, e1842531 (2021).
- ³³K. Tonokura and T. Suzuki, "Slicing photofragment spatial distribution by laser sheet ionization," *Chem. Phys. Lett.* **224**, 1–6 (1994).
- ³⁴K. Mizuse, R. Fujimoto, and Y. Ohshima, "Space-slice ion imaging: High slice resolution imaging in the polarization plane of arbitrarily polarized ionizing light," *Rev. Sci. Inst.* **90**, 103107 (2019).
- ³⁵H. Offerhaus, C. Nicole, F. Lepine, C. Bordas, F. Rosca-Pruna, and M. Vrakking, "A magnifying lens for velocity map imaging of electrons and ions," *Rev. Sci. Inst.* **72**, 3245–3248 (2001).
- ³⁶D. J. Harding, J. Neugeboren, D. J. Auerbach, T. Kitsopoulos, and A. M. Wodtke, "Using ion imaging to measure velocity distributions in surface scattering experiments," *J. Phys. Chem. A* **119**, 12255–12262 (2015).
- ³⁷T. Greenwood and S. P. K. Koehler, "Nitric oxide scattering off graphene using surface-velocity map imaging," *J. Phys. Chem. C* **125**, 17853–17860 (2021), <https://doi.org/10.1021/acs.jpcc.1c05014>.
- ³⁸D. J. Harding, J. Neugeboren, H. Hahn, D. Auerbach, T. Kitsopoulos, and A. M. Wodtke, "Ion and velocity map imaging for surface dynamics and kinetics," *J. Chem. Phys.* **147**, 013939 (2017).
- ³⁹J. Neugeboren, D. Borodin, H. W. Hahn, J. Altschäffel, A. Kandratsenka, D. J. Auerbach, C. T. Campbell, D. Schwarzer, D. J. Harding, A. M. Wodtke, and T. N. Kitsopoulos, "Velocity-resolved kinetics of site-specific carbon monoxide oxidation on platinum surfaces," *Nature* **558**, 280–283 (2018).
- ⁴⁰D. Borodin, I. Rahinov, O. Galparsoro, J. Fingerhut, M. Schwarzer, K. Golibruch, G. Skoulatakis, D. J. Auerbach, A. Kandratsenka, D. Schwarzer, T. N. Kitsopoulos, and A. M. Wodtke, "Kinetics of NH₃ desorption and diffusion on Pt: Implications for the ostwald process," *J. Am. Chem. Soc.* **143**, 18305–18316 (2021), PMID: 34672570, <https://doi.org/10.1021/jacs.1c09269>.
- ⁴¹D. Borodin, K. Golibruch, M. Schwarzer, J. Fingerhut, G. Skoulatakis, D. Schwarzer, T. Seelmann, T. Kitsopoulos, and A. M. Wodtke, "Measuring transient reaction rates from non-stationary catalysts," *ACS Catalysis* **10**, 14056–14066 (2020), PMID: 33343999, <https://doi.org/10.1021/acscatal.0c03773>.
- ⁴²E. Lundgren, C. Zhang, L. R. Merte, M. Shipilin, S. Blomberg, U. Hejral, J. Zhou, J. Zetterberg, and J. Gustafson, "Novel in situ techniques for studies of model catalysts," *Accounts of Chemical Research* **50**, 2326–2333 (2017).
- ⁴³M. A. van Spronsen, J. W. Frenken, and I. M. Groot, "Surface science under reaction conditions: CO oxidation on Pt and Pd model catalysts," *Chemical Society Reviews* **46**, 4347–4374 (2017).
- ⁴⁴M. A. Newton, "Time resolved operando x-ray techniques in catalysis, a case study: CO oxidation by O₂ over Pt surfaces and alumina supported Pt catalysts," *Catalysts* **7**, 58 (2017).
- ⁴⁵D. Starr, Z. Liu, M. Hävecker, A. Knop-Gericke, and H. Bluhm, "Investigation of solid/vapor interfaces using ambient pressure x-ray photoelectron spectroscopy," *Chemical Society Reviews* **42**, 5833–5857 (2013).
- ⁴⁶J. Schnadt, J. Knudsen, and N. Johansson, "Present and new frontiers in materials research by ambient pressure x-ray photoelectron spectroscopy," *Journal of Physics: Condensed Matter* **32**, 413003 (2020).
- ⁴⁷D. F. Ogletree, H. Bluhm, G. Lebedev, C. S. Fadley, Z. Hussain, and M. Salmeron, "A differentially pumped electrostatic lens system for photoemission studies in the millibar range," *Rev. Sci. Inst.* **73**, 3872–3877 (2002).
- ⁴⁸J. Knudsen, J. N. Andersen, and J. Schnadt, "A versatile instrument for ambient pressure x-ray photoelectron spectroscopy: The lund cell approach," *Surface Science* **646**, 160–169 (2016).
- ⁴⁹P. Amann, D. Degerman, M.-T. Lee, J. D. Alexander, M. Shipilin, H.-Y. Wang, F. Cavalca, M. Weston, J. Gladh, M. Blom, *et al.*, "A high-pressure x-ray photoelectron spectroscopy instrument for studies of industrially relevant catalytic reactions at pressures of several bars," *Rev. Sci. Inst.* **90**, 103102 (2019).
- ⁵⁰C. Papp and H.-P. Steinrück, "In situ high-resolution x-ray photoelectron spectroscopy—fundamental insights in surface reactions," *Surface science reports* **68**, 446–487 (2013).
- ⁵¹E. A. Redekop, N. Johansson, E. Kokkonen, S. Urpelainen, F. Lopes da Silva, M. Kaipio, H.-E. Nieminen, F. Rehman, V. Miikkulainen, M. Ritala, and U. Olsbye, "Synchronizing gas injections and time-resolved data acquisition for perturbation-enhanced apxps experiments," *Rev. Sci. Inst.* **92**, 044101 (2021).
- ⁵²J. Knudsen, T. Gallo, V. Boix, M. D. Strømsheim, G. D'Acunto, C. Goodwin, H. Wallander, S. Zhu, M. Soldemo, P. Lömker, *et al.*, "Stroboscopic operando spectroscopy of the dynamics in heterogeneous catalysis by event-averaging," *Nature communications* **12**, 1–8 (2021).
- ⁵³S. Blomberg, J. Zetterberg, J. Gustafson, J. Zhou, C. Brackmann, and E. Lundgren, "Comparison of AP-XPS and PLIF measurements during CO oxidation over Pd single crystals," *Topics in Catalysis* **59**, 478–486 (2016).
- ⁵⁴M. A. Tesa-Serrate, E. J. Smoll Jr, T. K. Minton, and K. G. McKendrick, "Atomic and molecular collisions at liquid surfaces," *Ann. Rev. Phys. Chem.* **67**, 515–540 (2016).
- ⁵⁵E. J. Smoll Jr and T. K. Minton, "Scattering-angle randomization in nonthermal gas–liquid collisions," *J. Phys. Chem. C* **123**, 22887–22896 (2019).
- ⁵⁶G. M. Nathanson, "Molecular beam studies of gas-liquid interfaces," *Annu. Rev. Phys. Chem.* **55**, 231–255 (2004).
- ⁵⁷A. Zutz and D. J. Nesbitt, "Angle-resolved molecular beam scattering of no at the gas-liquid interface," *J. Chem. Phys.* **147**, 054704 (2017).
- ⁵⁸E. J. Smoll Jr, S. M. Purcell, L. D'Andrea, J. M. Slattery, D. W. Bruce, M. L. Costen, K. G. McKendrick, and T. K. Minton, "Probing conformational heterogeneity at the ionic liquid–vacuum interface by reactive-atom scattering," *J. Phys. Chem. Lett.* **10**, 156–163 (2018).
- ⁵⁹R. H. Bianchini, M. J. Roman, M. L. Costen, and K. G. McKendrick, "Real-space laser-induced fluorescence imaging applied to gas-liquid interfacial scattering," *J. Chem. Phys.* **151**, 054201 (2019).
- ⁶⁰J. R. Roscioli and D. J. Nesbitt, "Quantum state resolved velocity-map imaging spectroscopy: A new tool for collision dynamics at gas/self-assembled monolayer interfaces," *Faraday Discussions* **150**, 471–479 (2011).
- ⁶¹C. H. Hoffman and D. J. Nesbitt, "Quantum state resolved 3d velocity map imaging of surface-scattered molecules: Incident energy effects in hcl+ self-assembled monolayer collisions," *J. Phys. Chem. C* **120**, 16687–16698 (2016).
- ⁶²A. Zutz, K. A. Peterson, and D. J. Nesbitt, "Nonadiabatic dynamics at the gas–molten metal interface: State-to-state resolved scattering of no from hot gallium (600–1000 k)," *J. Phys. Chem. C* **125**, 341–353 (2020).
- ⁶³M. Faubel, S. Schlemmer, and J. Toennies, "A molecular beam study of the evaporation of water from a liquid jet," *Z. Phys. D Atoms, Molecules and Clusters* **10**, 269–277 (1988).

- ⁶⁴M. Ryazanov and D. J. Nesbitt, “Quantum-state-resolved studies of aqueous evaporation dynamics: No ejection from a liquid water microjet,” *J. Chem. Phys.* **150**, 044201 (2019).
- ⁶⁵J. A. Faust, T. B. Sobyra, and G. M. Nathanson, “Gas–microjet reactive scattering: Collisions of hcl and dcl with cool salty water,” *J. Phys. Chem. Lett.* **7**, 730–735 (2016).
- ⁶⁶X. Kong, P. U. Andersson, E. S. Thomson, and J. B. Pettersson, “Ice formation via deposition mode nucleation on bare and alcohol-covered graphite surfaces,” *J. Phys. Chem. C* **116**, 8964–8974 (2012).
- ⁶⁷S. M. Johansson, X. Kong, P. Papagiannakopoulos, E. S. Thomson, and J. B. Pettersson, “A novel gas-vacuum interface for environmental molecular beam studies,” *Rev. Sci. Inst.* **88**, 035112 (2017).
- ⁶⁸S. M. Johansson, J. Lovrić, X. Kong, E. S. Thomson, P. Papagiannakopoulos, S. Briquez, C. Toubin, and J. B. C. Pettersson, “Understanding water interactions with organic surfaces: environmental molecular beam and molecular dynamics studies of the water–butanol system,” *Phys. Chem. Chem. Phys.* **21**, 1141–1151 (2019).
- ⁶⁹M. Faubel, B. Steiner, and J. P. Toennies, “Photoelectron spectroscopy of liquid water, some alcohols, and pure nonane in free micro jets,” *J. Chem. Phys.* **106**, 9013–9031 (1997).
- ⁷⁰R. Seidel, B. Winter, and S. E. Bradforth, “Valence electronic structure of aqueous solutions: Insights from photoelectron spectroscopy,” *Ann. Rev. Phys. Chem.* **67**, 283–305 (2016).
- ⁷¹R. Dupuy, C. Richter, B. Winter, G. Meijer, R. Schlögl, and H. Bluhm, “Core level photoelectron spectroscopy of heterogeneous reactions at liquid–vapor interfaces: Current status, challenges, and prospects,” *J. Chem. Phys.* **154**, 060901 (2021).
- ⁷²S. Malerz, H. Haak, F. Trinter, A. B. Stephansen, C. Kolbeck, M. Pohl, U. Hergenbahn, G. Meijer, and B. Winter, “A setup for studies of photoelectron circular dichroism from chiral molecules in aqueous solution,” *Rev. Sci. Inst.* **93**, 015101 (2022).
- ⁷³J. Long, Z. Qiu, J. Wei, D. Li, X. Song, B. Jin, and B. Zhang, “Liquid-microjet photoelectron imaging spectrometry for liquid aqueous solutions,” *Rev. Sci. Inst.* **92**, 065108 (2021).
- ⁷⁴O. Bünermann, H. Jiang, Y. Dorenkamp, A. Kandratsenka, S. M. Janke, D. J. Auerbach, and A. M. Wodtke, “Electron-hole pair excitation determines the mechanism of hydrogen atom adsorption,” *Science* **350**, 1346–1349 (2015), <https://www.science.org/doi/pdf/10.1126/science.aad4972>.
- ⁷⁵H. Jiang, M. Kammler, F. Ding, Y. Dorenkamp, F. R. Manby, A. M. Wodtke, T. F. Miller, A. Kandratsenka, and O. Bünermann, “Imaging covalent bond formation by h atom scattering from graphene,” *Science* **364**, 379–382 (2019), <https://www.science.org/doi/pdf/10.1126/science.aaw6378>.
- ⁷⁶S. Malerz, H. Haak, F. Trinter, A. B. Stephansen, C. Kolbeck, M. Pohl, U. Hergenbahn, G. Meijer, and B. Winter, “A setup for studies of photoelectron circular dichroism from chiral molecules in aqueous solution,” *Rev. Sci. Inst.* **93**, 015101 (2022), <https://doi.org/10.1063/5.0072346>.
- ⁷⁷M. Reid and S. P. K. Koehler, “Validation of velocity map imaging conditions over larger areas,” *Rev. Sci. Inst.* **84**, 044101 (2013), <https://doi.org/10.1063/1.4798646>.
- ⁷⁸T. F. Hanisco and A. C. Kummel, “State-resolved photodissociation of nitrous oxide,” *J. Phys. Chem.* **97**, 7242–7246 (1993).
- ⁷⁹T. Suzuki, H. Katayanagi, Y. Mo, and K. Tonokura, “Evidence for multiple dissociation components and orbital alignment in 205 nm photodissociation of N₂O,” *Chem. Phys. Lett.* **256**, 90–95 (1996).
- ⁸⁰D. W. Neyer, A. J. Heck, and D. W. Chandler, “Photodissociation of N₂O: J-dependent anisotropy revealed in N₂ photofragment images,” *J. Chem. Phys.* **110**, 3411–3417 (1999).
- ⁸¹T. Nishide and T. Suzuki, “Photodissociation of nitrous oxide revisited by high-resolution photofragment imaging: Energy partitioning,” *J. Phys. Chem. A* **108**, 7863–7870 (2004).
- ⁸²H. Kawamata, H. Kohguchi, T. Nishide, and T. Suzuki, “Photodissociation of nitrous oxide starting from excited bending levels,” *J. Chem. Phys.* **125**, 133312 (2006).
- ⁸³T. F. Hanisco and A. C. Kummel, “Resonantly enhanced multiphoton ionization of nitrogen a¹1. sigma. g+ (v’= v’). rarw. x1. sigma. g+ (v’= 0-2). 1. determination of rotational populations and virtual state character,” *J. Phys. Chem.* **95**, 8565–8574 (1991).
- ⁸⁴B. Baule, *Theoretische behandlung der erscheinungen in verdünnten gasen* (JA Barth, 1914).